Romanian Reports in Physics **XX**, XYZ (2024)

PHOTOLUMINESCENCE AND THERMO-STABILITY OF POLYMER COMPOSITE NANOMATERIAL $[Eu(\mu_2\text{-}OC_2H_5)(btfa)(NO_3)(phen)]_2\cdot phen/PEPC$

V. VERLAN[1], I. CULEAC[1]*, V. GHENEA[1,2], O. BORDIAN[1], V. ZUBAREVA[3], I. BULHAC[3], I. COJOCARU[1], M. ENACHESCU[4]

[1] Institute of Applied Physics, Moldova State University, MD2028 Chişinău, Republic of Moldova
E-mails: victor.verlan@ifa.usm.md; ion.culeac@ifa.usm.md; vladislav.ghenea@ifa.usm.md; olga.bordian@usm.md, ion.cojocaru@ifa.usm.md
[2] Technical University of Moldova, MD2004 Chişinău, Republic of Moldova
[3] Institute of Chemistry, Moldova State University, MD2028 Chişinău, Republic of Moldova,
E-mails: vera.zubareva@sti.usm.md, ion.bulhac@sti.usm.md
[4] Center for Surface Science and Nanotechnology, National University of Science and Technology POLITEHNICA Bucharest, 060042 Bucharest, Romania, E-mail: marius.enachescu@cssnt-upb.ro

Received

Abstract. Nanocomposite (NC) thin films based on a dinuclear coordination compound $[Eu(\mu_2\text{-}OC_2H_5)(btfa)(NO_3)(phen)]_2\cdot phen$ and poly-N-epoxypropylcarbazole (PEPC) have been obtained by chemical methods. Photoluminescence (PL) spectra of the NC reveal characteristic atomic-like narrow emission bands associated with internal *4f-4f* radiative transitions of Eu^{3+} ion, $^5D_{0,1}\rightarrow{}^7F_J$ *(J = 0–4)*. The excitation spectrum of the complex contains a broad band (≈ 300–500 nm) related to the matrix, as well as a number of narrow excitation bands, determined by the internal transitions within the Eu(III) ion (463.6, 532.4, 578 nm). Thermogravimetry analysis and differential scanning calorimetry of the NC show a tendency to higher thermal stability compared to the original complex, and almost the same PL radiative parameters. PL quenching appears at concentration of about 10%, as expected based on literature data. The pattern of excitation and emission spectra of the NC indicate that it can be effectively excited by a blue-light source 405 nm, which fits well existing cheap blue-light LED sources.

Key words: europium; coordination compound, composite, thermogravimetry analysis, photoluminescence; quantum yield.

1. INTRODUCTION

Lanthanide complexes possess a number of unique properties, which make them attractive for practical applications in optoelectronics [1-3], luminescent biosensing and biophotonics [4-7], electroluminescent devices [8], telecommunication [9,10], etc. Particularly the Eu^{3+} based coordination compounds keep a special place among the Ln complexes because of a series of their specific advantages: high PL efficiency and colour purity, a simple structure of the PL spectra, the possibility to be used as a spectroscopic probe, etc. Both the absorption

and luminescence spectra of the Eu^{3+} ion exhibit specific narrow transitions.

Eu^{3+}-based complexes display strong emission upon UV or blue-light irradiation owing to the sensitization of lanthanide ions by the coordinating ligands. Photoluminescence properties of Eu^{3+} coordination compounds, like all other lanthanide complexes, are basically determined by the *4f*-shell electrons, which are shielded by the outer electrons shell $5s^2$ and $5p^6$ from the crystal field [11,12]. Intramolecular energy transfer in the coordination compound occurs from the coordinating ligands to the localized intra-*4f* shell of the lanthanide ions, leading to luminescence with an enhanced quantum yield [13]. However, there is a problem with practical applications of the Ln complexes because of their poor thermal and mechanical properties. For various applications in optoelectronics there is a need of materials with high thermo-stability and high emission efficiency. One of possible ways to overcome these problems is to incorporate the Ln complex into a polymer matrix to obtain more stable composite material, which would be more convenient for practical applications [14,15]. The current research efforts are focused on achieving nanocomposite materials that would exhibit improved thermo-mechanical properties, compared to Eu^{3+} complexes, which are requested for practical applications in optoelectronics and biochemistry.

In the previous paper [16] we presented experimental results on a new dinuclear coordination compound with high luminescence efficiency $[Eu(\mu_2\text{-}OC_2H_5)(btfa)(NO_3)(phen)]_2\cdot phen$. In the present work we report a luminescent nanocomposite (NC) made of this coordination compound (CC) and an oligomer matrix of poly-N-epoxypropylcarbazole (PEPC), which shows good PL efficiency along with improved thermal stability.

2. MATERIALS AND METHODS

Synthesis of the complex $[Eu(\mu_2\text{-}OC_2H_5)(btfa)(NO_3)(phen)]_2\cdot phen$ was described elsewhere [16]. The chemical structure of the constituent components is illustrated in Fig. 1. The Eu^{3+} complex was successfully incorporated into organic matrixes of PEPC oligomer via sol–gel process. The nanocomposite $[Eu(\mu_2\text{-}OC_2H_5)(btfa)(NO_3)(phen)]_2\cdot phen$/PEPC was obtained from chemical solutions at different molar ratios of coordination compound into polymer matrix. PEPC polymer and polycrystals $[Eu(\mu_2\text{-}OC_2H_5)(btfa)(NO_3)(phen)]_2\cdot phen$ were dissolved in toluene by ultrasonic dispersing at room temperature.

The solution of the coordination compound of different concentrations (0.6%, 2.0%, 10%, 14.6%; 20%) was added to the polymer solution and the final composition was mixed using an ultrasonic bath. Deposition of the nanocomposite on quartz substrates was performed applying the spin-coating method. The samples

were dried at 80 °C for 2 hours. The dried layers with thicknesses around 1 μm are transparent in the visible range of the spectrum.

Fig. 2 shows the Tauc plot for the absorption spectra of nanocomposite films in the range 350–650 nm at different concentrations of Eu^{3+} complex. The absorption threshold, estimated from the Tauc plot was found to vary in the range 3.07–3.34 eV for different concentrations of coordination compound (0.6–20%). While increasing concentration of Eu^{3+} complex the absorption threshold shifts to infrared.

The Thermogravimetric Analysis (TGA) and Differential Scanning Calorimetry (DSC) of the nanocomposite were performed using the STA8000 PerkinElmer scanning system. The parameters used for the differential scanning were set as follows: the air transport flow rate 19.8 ml/min, temperature range 30–600 °C, temperature scan speed 10 °C/min, α-Al_2O_3 was used as a reference. The mass of the sample was 1.440 mg (powder with particle sizes smaller than 50 μm).

Photoluminescence characteristics were investigated at room temperature. Low resolution emission spectra (0.125 nm) were registered with an MDR-23 single grating monochromator (LOMO, St Petersburg, Russia) and a Hamamatsu photomultiplier head H9319-02-12 in a photon counting mode. High-resolution PL emission spectra (0.2 cm^{-1}) were registered with a double grating spectrophotometer DFS-52 (LOMO) and a Hamamatsu photomultiplier module H8259-01 in a photon counting mode. PL spectra were registered with a Thorlabs L375P70MLD Laser Diode (375 nm, 75 mW) as an excitation source. A pulsed nitrogen laser (337 nm) with a repetition rate of 10 Hz and a pulse width of 10 ns was used for the PL time decay measurements. The emitted light was detected with a module Hamamatsu H8259-01 and a counting unit C8855-01 connected to a PC. The excitation spectra were registered with an MDR-23 single grating monochromator as an excitation source and a double grating spectrometer DFS-52 for collecting the PL emission. A halogen lamp OSRAM 64623 HLX 12V 100W was used as a light excitation source. The spectra were corrected for the instrument spectral sensitivity.

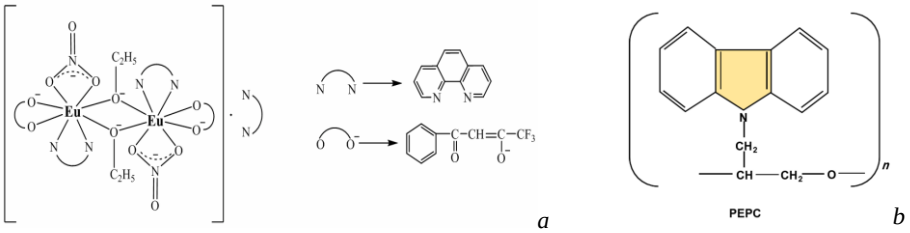

Fig. 1. Illustration of chemical structure of NC constituent components: (*a*) - the binuclear [Eu(μ_2-OC_2H_5)(btfa)(NO_3)(phen)]$_2$·phen compound [16]; (*b*) - poly-N-epoxypropylcarbazole (PEPC).

3. THERMOGRAVIMETRY ANALYSIS AND DIFFERENTIAL THERMOGRAVIMETRY CHARACTERIZATION

The TGA/DTG and DSC characteristics of the nanocomposite, registered in the temperature range 30–900 °C, are illustrated in Fig. 3. Some decomposition-degradation data are presented in Table 1. The process of thermal decomposition is complex and is accompanied by a number of endothermic and exothermic effects. In the temperature range 30–127.7 °C the TGA graph shows a horizontal line, without mass loss. This indicates the thermal stability of the nanocomposite in this range. The temperature value 127.7 °C is probably the starting point of softening and melting (volatility) of the PEPC matrix. As the temperature increases, the mass loss of PEPC occurs due to its evaporation and complete degradation by oxidation and subsequent removal from the system with the air flow. TGA indicates a mass loss of 7.0 % in this temperature range. According to the DSC plot this process is endothermic in the range 127.8–180.5 °C.

The following TGA stage registered in the range 180.5–327.5 °C shows a horizontal line which is attributed to the heating of the material, which remained after the removal of PEPC, and indicates the thermal stability of the Eu^{3+} complex in this range. The point T=327.5 °C appears as the temperature of softening (volatility) and melting of the compound. The DSC plot marks this process as endothermic with the maximum at 332.58 °C.

The thermolysis stage, which is registered in the temperature range 327.5–419.8 °C, is associated with decomposition of all the ligands, and elimination of ether, *phen*, NO_3, of the second ligand from the surrounding sphere of the Eu^{3+} ion. Finally, elimination of *btfa* occurs by breaking the chemical bonds with the Eu^{3+} ion and oxidizing them with the formation of gaseous compounds, which are removed together with the gas flow. Their decarboxylation takes place with an essential mass loss of 69.0% of the total mass. The DSC graph marks these processes as exothermic with the maximum at 353.1 °C.

In the following TGA temperature ranges, 419.8–479.8 °C and 479.8–555.9 °C, some oxidation and carbonization processes of the disintegrated material appear at mass losses of 3.3% and 12.8% with the formation of carbonized residue and europium oxide Eu_2O_3. The complete destruction and passage through several stages of the Eu^{3+} compound upon thermolysis is also observed on the DSC graph as an exothermic process with maxima at 381.3 °C, 413.8 °C and 521.3 °C. Finally, the TGA graph appears as a horizontal line, showing a steady state of carbonized remains and europium oxide. The mass loss is complete at 560 °C [17]. Table 1 illustrates some characteristic data on thermal degradation, derived from the TGA and DSC graphs in Fig. 2. Experimental data, listed in Table 1, indicate that thermal properties of the nanocomposite are high enough for the luminescence practical applications.

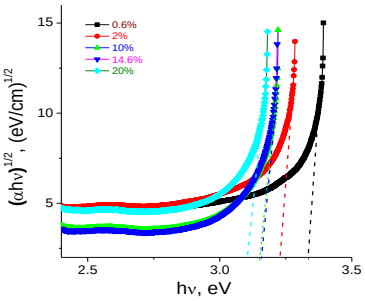

Fig. 2. Tauc plot for composite with different concentrations of the Eu^{3+} coordination compound.

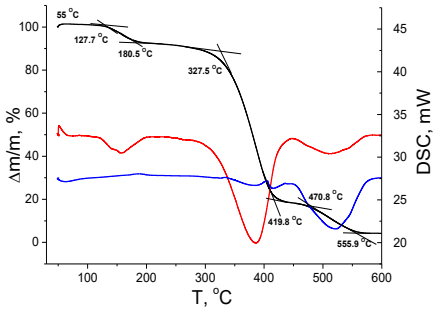

Fig. 3. TG/DTG analysis of the composite [Eu(μ2-OC_2H_5)(btfa)(NO_3)(phen)]2·phen/PEPC (20% of the complex).

Table 1

Thermal decomposition of the nanocomposite (20% of the Eu^{3+} complex).

Decomposition stage	Temperature range, °C	TGA range, %	DSC peaks, °C	Thermolysis process DSC
Water removal	30.0–55.0			
Heating of the nanocomposite	55.0–127.8	100.0–100.0	127.80	endo
Melting and degradation of PEPC by oxidation	127.8–180.5	100.0–93.0	186.50	endo
Heating of the remaining compound, beginning of melting	180.5–327.5	93.0–88.8	332.58	endo
Compound degradation	327.5–419.8	88.8–19.8	381.33	exo
Disintegration	419.8–479.8	19.8–16.5	413.83	exo
	479.8–555.9	16.5–3.7	521.30	exo

3. PHOTOLUMINESCENT CHARACTERISTICS

The excitation spectra of the complex and of the nanocomposite, are represented in Fig. 4. The excitation spectra were recorded in the range of 300–590 nm at room temperature, with the emission monitored in the $^5D_0 \rightarrow {}^7F_2$ transition of the Eu^{3+} ion at ~612 nm. The excitation spectrum of the complex exhibits a number of narrow absorption bands, related to Eu^{3+} *4f–4f* states transitions, and centred at 413.2 ($^7F_0 \rightarrow {}^5D_3$), 433.8 ($^7F_2 \rightarrow {}^5D_3$), 463.5 ($^7F_0 \rightarrow {}^5D_2$), 471.8 ($^7F_0 \rightarrow {}^5D_1$), 533.4 ($^7F_1 \rightarrow {}^5D_1$), 578.3 ($^7F_0 \rightarrow {}^5D_0$) nm, respectively. The broad band in the range from 300 to 475 nm arises from the π-π^* ($S_0 \rightarrow S_1$) transitions. This broad band overlaps with the narrow bands arising from the Eu^{3+} ion internal transitions $^7F_0 \rightarrow {}^5D_3$, $^7F_2 \rightarrow {}^5D_3$.

The excitation spectrum of the nanocomposite bears the same features as the excitation spectrum of the original complex (Fig. 4). Both the spectra exhibit a wide absorption band in the range 300–475 nm, along with a number of narrow absorption bands, ascribes to Eu^{3+} excited states 463.5 ($^7F_0 \rightarrow {}^5D_2$), 533.4 ($^7F_1 \rightarrow {}^5D_1$), 578.3 ($^7F_0 \rightarrow {}^5D_0$) nm, respectively. In the case of NC, the absorption bands, related to optical transitions of the Eu^{3+} ion, are less intensive. The broad band associated with the π-π^* transitions is shifted in the NC to infrared, with the peak shifting from ~375 to about 402 nm, which could be ascribed to PEPC polymer absorption.

The position of the excitation peak ($S_0 \rightarrow S_1$) in the NC sample at ca 402 nm correlates with the NC bandgap, of the corresponding sample (20%), estimated from the Tauc plot in Fig. 2. The pattern of the excitation spectrum of the NC indicates that π-π^* transition, followed by intramolecular energy transfer, is the most effective excitation pathway responsible for the PL emission [18].

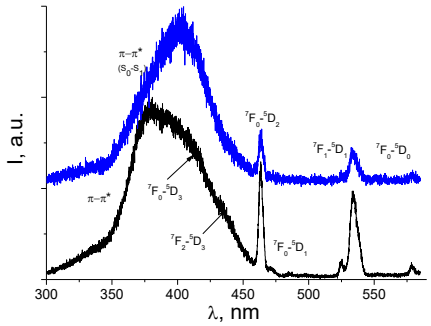

Fig. 4. Excitation spectrum of the Eu(III) complex (black), and of NC sample 20% (blue).

The emission spectra were registered under a laser excitation wavelength of 405 nm, which perfectly matches the excitation spectrum of the NC (Fig. 4). The PL emission spectra of the Eu^{3+} NC nanocomposite display a number of narrow bands, assigned to internal transitions between *4f–4f* excited states transitions of the Eu(III) ion, $^5D_{0,1}$ and the ground multiplet $^7F_{0\text{-}4}$.

The spectra bear the same characteristic features as the original Eu^{3+} complex. The NC sample shows a number of metal-centred emission bands, which are characteristic for Eu^{3+} ion. The main PL emission bands are positioned in a relatively wide range 570–720 nm (Fig. 5) and correspond to internal radiative transitions of the Eu^{3+} ion, $^5D_0 \rightarrow {}^7F_J$. The barycenters of these transitions are found at 579.2, 590.4, 612.9, 652, and 694.4 nm respectively. The dominant emission band of the NC sample, similarly to the Eu^{3+} complex, is the electric dipole transition $^7F_0 \rightarrow {}^5D_2$.

The low-resolution emission spectra of the NC, for different concentrations of the Eu^{3+} complex, are represented in Fig. 5. While increasing the concentration of the Eu^{3+} complex up to about 10% there is a gradual increase in PL emission intensity (Fig. 5, insert), but further increase of the concentration leads to quenching of the PL emission. The quenching effect can be associated with decreasing the average distance and energy migration between the ions. In the case of Eu^{3+} the critical distance between the ions, when quenching effect appears, is estimated to be reached at concentrations of tens of percent [19]. This critical distance between Eu^{3+} ions satisfy the Dexter and Forster resonant energy transfer condition [20].

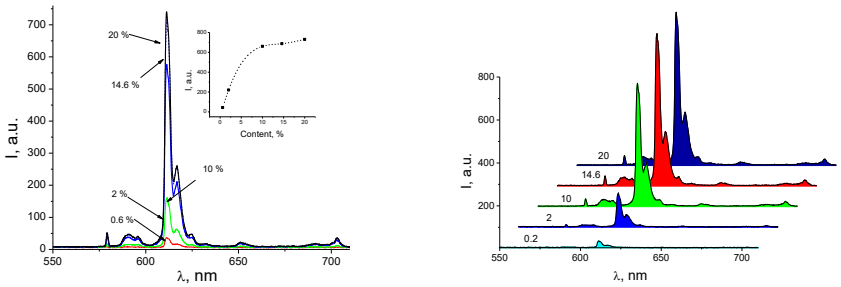

Fig. 5. Low-resolution emission spectra of the of the NC [Eu(μ$_2$-OC_2H_5)(btfa)(NO_3)(phen)]$_2$·phen/PEPC for different concentrations of the Eu^{3+} complex.

Low-resolution emission spectrum of the original Eu^{3+} complex is represented in Fig. 6. In the case of the Eu^{3+} complex we can distinguish the dominant emission band $^5D_0 \rightarrow {}^7F_2$ splitting into at least six components, while the maximum number of $2J+1$ components of this transition for a single Eu^{3+} site is five. Consequently, registration of more components for this transition, than the maximum possible number ($2J+1$) is another indication of existing of two different sites of the Eu^{3+} ion [16]. Notable, in the case of NC spectra, the $^7F_0 \rightarrow {}^5D_2$ band splitting is less distinguished, although it exhibits similarly to the original complex a splitting into at least six components. This points to the existence of two different sites of the Eu^{3+} in the matrix of the nanocomposite, similar to original Eu^{3+} complex.

The electric-dipole transition $^5D_0 \rightarrow {}^7F_2$ of Eu^{3+} ion is known as a "hypersensitive" one, which means that its intensity is more sensitive to the local environment in which the Eu^{3+} ion is located, compared to other electric-dipole transitions. Therefore, the pattern of the emission spectrum may provide some information about the microstructure of the complex. Specifically, the dominance of the electric-dipole transition $^5D_0 \rightarrow {}^7F_2$ suggests two possible explanations: (*i*) that the Eu^{3+} is at a site without an inversion centre, or (*ii*) a highly polarizable

ligand environment around the Eu^{3+} ion [13,21]. Because no ligand phosphorescence was registered in the PL spectra, this can be considered as an indication of an efficient energy transfer from the ligand to the Eu^{3+}ion.

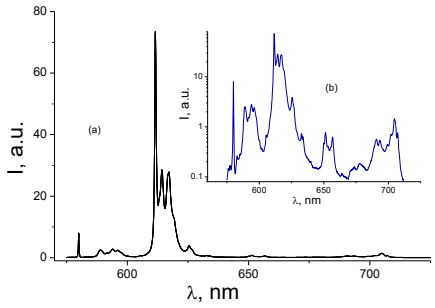

Fig. 6. Low-resolution emission spectrum of the of the Eu^{3+} complex. The inset represents the plot in a logarithmic scale.

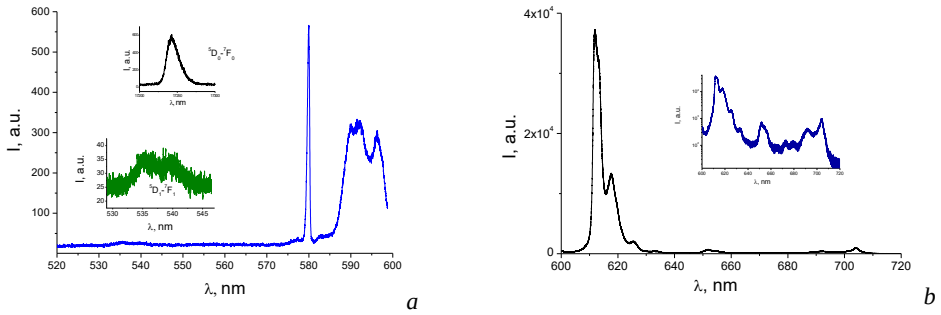

Fig. 7. High-resolution spectra of the transitions $^5D_0 \rightarrow {}^7F_{0,1}$ (*a*) and $^5D_0 \rightarrow {}^7F_{2,3,4}$ (*b*) for the NC sample 20% (T = 300 K).

The splitting pattern of the nanocomposite band $^5D_0 \rightarrow {}^7F_1$ (Fig. 7) shows the presence of at least four components for the $^5D_0 \rightarrow {}^7F_1$ transition, which suggests, that the Eu^{3+} is in a site with low symmetry [13,21,22]. Five components that are due to the Stark splitting of the $^7F_1$ level arise from two sites of the europium ion Eu^{3+} in the coordination compound.

The asymmetry ratio $R = I(^5D_0 \rightarrow {}^7F_2)/I(^5D_0 \rightarrow {}^7F_1)$ is dependent on the type and coordination of the ligands around the Eu^{3+} ion [13]. In the case of the nanocomposite sample (Fig. 8) the asymmetry ratio is R = 9.38, compared to R = 10.6 for the Eu^{3+} complex. The asymmetry ratio is considered an indicator of Eu^{3+} site symmetry, and a measure of the extent of Eu^{3+} interaction with surrounding ligands [23,24]. Commonly, but not necessarily, the higher the value of R is, the lower is the symmetry of the Eu^{3+} ions site [21]. When the Eu^{3+} ion is situated in a

low symmetry site, without inversion centre, the hypersensitive transition $^5D_0 \rightarrow {}^7F_2$ is often dominating in the emission spectra [25]. Although, high asymmetry ratio may be related to high polarizability of the ligands [13,21].

The $^5D_0 \rightarrow {}^7F_0$ transition is a forbidden one by forced electric dipole mechanism, and its appearance in the PL spectrum is explained by the *J*-mixing of $^7F_0$ with $^7F_2$ state [21,26,27]. Observation of $^5D_0 \rightarrow {}^7F_0$ transition is commonly considered as an indicator of low symmetry complex [13].

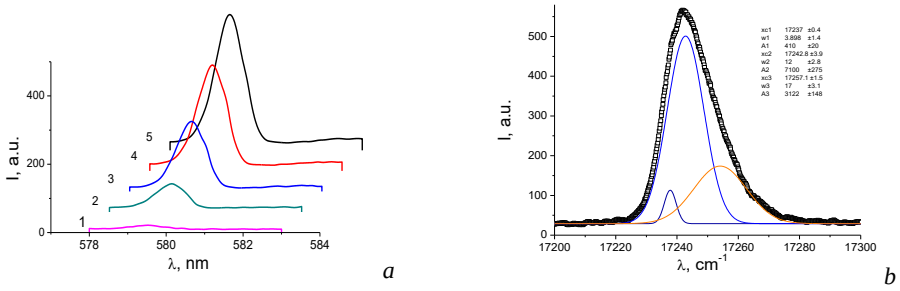

Fig. 8. Nanocomposite PL emission spectra of the transition $^5D_0 \rightarrow {}^7F_0$: *a* - low resolution spectra of the transition at different concentrations: 1 - 0.6%; 2 - 2%; 3 - 10%; 4 - 14.6%; 5 - 20%; *b* - high-resolution spectrum of the transition (NC sample, 20% of the complex).

The $^5D_0 \rightarrow {}^7F_0$ transition is a forbidden one by forced electric dipole mechanism, and its appearance in the PL spectrum is explained by the *J*-mixing of $^7F_0$ with $^7F_2$ state [21,26,27]. Observation of $^5D_0 \rightarrow {}^7F_0$ transition is commonly considered as an indicator of low symmetry complex [13].

Another feature to be noted in the emission spectra of the NC is the asymmetry of the $^5D_0 \rightarrow {}^7F_0$ band (Fig. 8), which directly suggests that $^5D_0 \rightarrow {}^7F_0$ transition contains two components. Indeed, the high-resolution spectrum of this transition reveals two ultra-narrow components for $^5D_0 \rightarrow {}^7F_0$ band (Fig. 8, *b*). In the case of NC the full width at half maximum (FWHM) of this transition at room temperature was determined to be ca. 20 cm^{-1}. This value is about as twice as large than the corresponding value of FWHM for the coordination complex (ca. 12 cm^{-1}). Since both the initial and final level of the transition $^5D_0 \rightarrow {}^7F_0$ are nondegenerate, the number of component lines indicate the number of different Eu^{3+} ion sites in the complex [28].

5. RADIATIVE PARAMETERS

The Judd–Ofelt theory [29,30] has been applied to evaluate some radiative parameters of the Eu^{3+} complex from PL emission spectra, such as radiative transition probability $A_{rad}(J)$, radiative decay time τ_{rad}, luminescence branching

ratios β_{0J}, as well as the intensity parameters Ω_2 and Ω_4 (Table 2). The radiative transition probability $A_{rad}(J)$ can be expressed as follows [13,31-33]:

$$A_{rad}(J) = \frac{64\pi^4 \tilde{\upsilon}^3}{3h(2J+1)}\left[\frac{n\left(n^2+2\right)^2}{9} D_{ed} + n^3 D_{md}\right] \quad (1)$$

where $\tilde{\upsilon}$ is the average wavenumber of the transition (cm^{-1}), D_{ed} and D_{md} are the electric and magnetic dipole line strengths, J is the total angular momentum of the ground state, h is the Planck constant, and n is the refractive index.

The intensity parameter Ω_2, determined by the intensity of electric-dipole transition, is known to be related to the covalence and/or structural changes in the vicinity of the Eu^{3+} ion, while Ω_4 is related to long-range effects [29,30]. The large value of the parameter Ω_2 indicates the presence of covalent bonding between the central lanthanide ion and the surrounding ligands [34].

Table 2
Experimental parameters of the nanocomposite at 300 K

Transition	$^5D_0\rightarrow{}^7F_0$		$^5D_0\rightarrow{}^7F_1$		$^5D_0\rightarrow{}^7F_2$		$^5D_0\rightarrow{}^7F_3$		$^5D_0\rightarrow{}^7F_4$	
	CC	NC	CC	NC	CC	NC	CC	NC	CC	NC
Barycenter, $\lambda_{0\text{-}J}$, nm	579.96	579.2	593.65	592.4	614.65	612.9	653.3	652.0	701.28	694.4
$I(^5D_0\rightarrow{}^7F_J)/I(^5D_0\rightarrow{}^7F_1)$	0.1439	0.165	1	1	10.607	9.379	0.1919	0.315	0.5217	0.709
$A_{rad}(J)$, s^{-1}	7.03	8.05	50	50	549.14	485.18	10.506	17.36	30.816	41.54
β_{0J}, % (exp)	1.09	1.34	7.72	8.30	84.81	80.78	1.62	2.88	4.56	6.89
β_{0J}, % (calc)	-	-	7.94	8.67	87.17	84.13	-	-	4.89	7.20
Ω_λ, cm^2	-	-	-	-	17.13×10^{-20}	15.12×10^{-20}	-	-	1.74×10^{-20}	2.31×10^{-20}

The emission lifetimes were obtained from analyses of the luminescence decay profile, which was monitored at 612 nm in the NC sample under laser pulse excitation 337 nm (Fig. 9). The PL decay can be fitted by two-exponential function:

$$I(t) = A_1 \exp\left(-t/\tau_1\right) + A_2 \exp\left(-t/\tau_2\right) \quad (2)$$

where A_1 and A_2 are pre-exponential factors, τ_1 and τ_2 are the time constants. The time decay constants obtained from the plot in Fig. 9 are τ_1 = 0.50 ms, and τ_2 = 0.61 ms respectively. The character of measured luminescence decay profile of the $^5D_0\rightarrow{}^7F_2$ transition is bi-exponential, suggesting the existence of two non-equivalent, nearly identical coordination environments of Eu^{3+} in the matrix. This bi-exponential character of PL decay can be associated with two different excited

species of Eu^{3+} or with energy back transfer from the metal to the triplet state of the organic ligand [35].

The measured decay profile can be used for the evaluation of the intrinsic quantum yield Q_{Eu}. The observed luminescence lifetime τ_{obs} of the $^5D_0$ excited state can be taken as the average of the time constants τ_1 and τ_2. The average lifetime τ_{av}, evaluated from the PL decay curve of the NC sample, is obtained from the relation [36,37]:

$$\tau_{av} = \left(A_1\tau_1^2 + A_2\tau_2^2\right)/\left(A_1\tau_1 + A_2\tau_2\right) \quad (3)$$

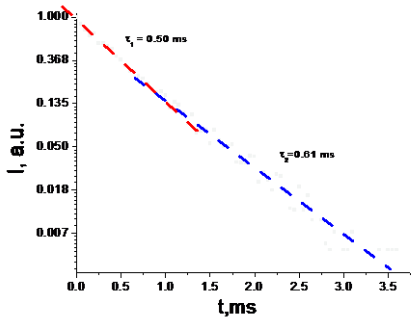

Fig. 9. The PL decay of NC sample 20% monitored at 612 nm under excitation of laser pulse 337 nm (the average of 10 pulses).

The average lifetime τ_{av} calculated from relation (3) is found to be equal to 0.56 ms. The radiative decay time τ_{rad} for the Eu^{3+} ions is calculated from the PL emission spectrum based on the Judd–Ofelt approach and the magnetic dipole nature of $^5D_0 \rightarrow {}^7F_1$ transition [13,38]:

$$\frac{1}{\tau_r} = A_{MD} n^3 \left(\frac{I_T}{I_{MD}}\right) \quad (4)$$

where A_{MD} is the known probability of spontaneous emission for $^5D_0 \rightarrow {}^7F_1$ transition, equal to 14.65 s^{-1}; I_T is the total integrated intensity of the emission spectrum; I_{MD} is the integrated intensity of the magnetic dipole transition; and n is the refractive index of the matrix taken to be 1.5 [39]. The radiative lifetime τ_{rad} calculated from (4) is found to be 1.72 ms. The intrinsic quantum yield Q_{Eu} is estimated from the relation (5), which defines the ratio of the observed luminescence lifetime τ_{obs} and the radiative lifetime τ_{rad} [40]:

$$Q = \tau_{obs} / \tau_{rad} \quad (5)$$

The intrinsic quantum yield of the nanocomposite, calculated from (5) is found to be 32.7%, compared to 55.1%, which was reported for original complex in [16]. The radiative parameters of the NC are commensurable with corresponding values of the original Eu^{3+} dinuclear complex.

CONCLUSIONS

Nanocomposite thin films based on a dinuclear coordination compound $[Eu(\mu_2\text{-}OC_2H_5)(btfa)(NO_3)(phen)]_2 \cdot phen$ and poly-N-epoxypropylcarbazole have been obtained by chemical methods. PL emission spectra of the nanocomposite reveal characteristic atomic-like narrow emission bands associated with internal 4*f*–4*f* radiative transitions of Eu^{3+} ion $^5D_0 \rightarrow {}^7F_J$ ($J = 0–4$). The excitation spectrum of the nanocomposite exhibits a broad band (~300–500 nm) related to matrix absorption, along to a number of narrow absorption bands, determined by the transitions within the Eu^{3+} ion (463.6, 532.4, 578 nm).

TGA/DSC measurements show a tendency of nanocomposite for improvement in the aspect of thermal stability compared to the original complex, and almost the same PL radiative parameters, although it shows a slightly lower emission quantum efficiency.

Variation in the PL emission intensity with Eu^{3+} complex concentrations shows that PL quenching appears at concentration of about 10%, as expected based on literature data. Compared to coordination compound, the broad band in the excitation spectrum of the nanocomposite, associated with the π-π^* transitions, is shifted to infrared, from ~375 to ~402 nm. The pattern of excitation and emission spectra of the nanocomposite indicates that it can be effectively excited by a blue-light source (405 nm), which excellently fits existing cheap blue-light LED sources. TGA experimental data, indicate that thermal properties of the nanocomposite are high enough for the luminescence practical applications.

Acknowledgements. This research was funded by the Ministry of Education and Research of the Republic of Moldova (subprograms 011201, 010602), as well as by Chips Joint Undertaking under the following grant agreements: no. 101112338 (R-PODID), no. 101096772 (14ACMOS) and no. 101097296 (HICONNECTS). Chips Joint Undertaking. R-PODID, 14ACMOS and HICONNECTS projects are supported by Chips Joint Undertaking and its members, including the top-up funding of Italy, Turkey, Portugal, The Netherlands, Czech Republic, Latvia, Greece, and Romania Belgium, Germany, Israel, Austria, Finland, Sweden, France, Denmark, and Greece. This work is financially supported by the Romanian Ministry of Research, Innovation and Digitalization, under the PNRR-C9-I8 project "Novel Graphene/metal composites as advanced catalytic systems in the hydrogen based energetics", contract no. 760087/23.05.2023.

REFERENCES

1. A. P. Demchenko, *Introduction to Fluorescence Sensing*, Springer Cham, 794 p. (2015).

2. Y.-W. Zhao, F.-Q. Zhang, and X.-M. Zhang, ACS Appl. Mater. Interfaces **8**, 24123–24130 (2016).
3. D. Yang, Y. Xu, Y. Yao, J. Zhang, J. Wang, and Y. Wang, Synth. Metals **221**, 236–241 (2016).
4. P. Escribano, B. Julián-López, J. Planelles-Aragó, E. Cordoncillo, B. Viana, and C. Sanchez, J. Mater. Chem. **18**, 23–40 (2008).
5. S. V. Eliseeva and J.-C. G. Bunzli, Chem. Soc. Rev. **39**, 189–227 (2010).
6. G. R. Motson, J. S. Fleming, and S. Brooker, Adv. Inorg. Chem. **55**, 361–432 (2004).
7. Y. Zhao, Z. Yao, C. D. Snow, Y. Xu, Y. Wang, D. Xiu, L. A. Belfiore, and J. Tang, Nanomaterials **11**, 2462 (2021).
8. J. Kido, W. Ikeda, M. Kimura, and K. Nagai, Jpn. J. Appl. Phys. **35**, L394–L396 (1996).
9. J. R. Lakowicz, *Principles of Fluorescence Spectroscopy*, Springer, New York, 954 p. (2006).
10. R. Hull, J. Parisi, R. M. Osgood, H. Warlimont, G. Liu, and B. Jacquier, *Spectroscopic properties of rare earths in optical materials*, Springer, Berlin, Heidelberg, 550 p. (2005).
11. P. A. Tanner, *Lanthanide luminescence in solids*. P. Hanninen and H. Harma (Eds.), *Lanthanide luminescence, photophysical, analytical and biological aspects*, Springer, Berlin, Heidelberg, pp. 183–233 (2011).
12. H.-T. Wong, H. L. W. Chan, and J. H. Haoa, Appl. Phys. Lett. **95**, 022512 (2009).
13. K. Binnemans, Coordin. Chem. Rev. **295**, 1–45 (2015).
14. D. Yang, J. Wang, and H. Li, Dyes Pigm. **118**, 53–57 (2015).
15. V. I. Verlan, M. S. Iovu, I. Culeac, Y. Nistor, C. I. Turta, V. E. Zubareva, and S. Buzurniuc, J. Non. Cryst. Solids **357**, 1004–1007 (2011).
16. I. P. Culeac, V. I. Verlan, O. T. Bordian, V. E. Zubareva, M. S. Iovu, I. I. Bulhac, N. A. Siminel, A. V. Siminel, G. Mihai, and M. Enachescu, Nanomaterials **12**, 2788 (2022).
17. P. J. Haines, *Principles of thermal analysis and calorimetry*, Royal Society of Chemistry, 220 p. (2002).
18. C. V. Rodrigues, L. L. Luz, J. D. L. Dutra, S. A. Junior, O. L. Malta, C. C. Gatto, H. C. Streit, R. O. Freire, C. Wickleder, and M. O. Rodrigues, Phys. Chem. Chem. Phys. **16**, 14858–14866 (2014).
19. Z. Wang, *Multi-photon processes in lanthanide-doped nanocrystals*. PhD thesis, Utrecht University (2019).
20. T. Linda Francis, R. P. Prabhakar, T. Mariyam, S. K. Mahesh, V. R. Reshmi, and T. S. Sreena, Phys. Chem. Chem. Phys. **16**, 17108–17115 (2014).
21. P. A. Tanner, Chem. Soc. Rev. **42**, 5090–5101 (2013).
22. A. C. Coelho, A. C. Gomes, J. A. Fernandes, F. A. Almeida Paz, S. S. Braga, L. Rino, L. Pereira, M. Pillinger, and I. S. Gonçalves, Eur. J. Inorg. Chem. **2014**, 1284–1288 (2014).
23. K. Binnemans and C.Görller-Walrand, J. Rare Earths **14**, 173–180 (1996).
24. T. H. Q. Vu, B. Bondzior, D. Stefanska, N. Miniajluk, and P. J. Deren, Materials **13**, 1614 (2020).
25. M. G. Matos, P. S. Calefi, K. J. Ciuffi, and E. J. Nassar, Inorg. Chim. Acta **375**, 63–69 (2011).
26. P. Porcher and P. Caro, J. Lumin. **21**, 207–216 (1980).
27. M. Tanaka, G. Nishimura, and T. Kushida, Phys. Rev. B **49**, 16917–16925 (1994).
28. C. Gorller-Walrand and K. Binnemans, *Rationalization of crystal-field parametrization*. K. A. Gschneidner, Jr. and L. Eyring (Eds.), *Handbook on the Physics and Chemistry of Rare Earths V. 23*, Elsevier, pp 121–283 (1996).
29. B. R. Judd, Phys. Rev. **127**, 750–761 (1962).
30. G. S. Ofelt, J. Chem. Phys. **37**, 511–520 (1962).
31. M. H. V. Werts, R. T. F. Jukes, and J. W. Verhoeven, Phys. Chem. Chem. Phys. **4**, 1542–1548 (2002).
32. V. Lavin, P. Babu, C. K. Jayasankar, I. R. Martin, and V. D. Rodriguez, J. Chem. Phys. **115**, 10935–10944 (2001).
33. K. Swapna, S. K. Mahamuda, A. Srinivasa Rao, T. Sasikala, P. Perumal, L. Rama Moorthy, and G. Vijaya Prakash, J. Lumin. **156**, 80–86 (2014).

34. J. Feng and H. Zhang, Chem. Soc. Rev. **42**, 387–410 (2013).
35. P. E. Reiller and J. Brevet, Spectrochim. Acta A Mol. Biomol. Spectrosc. **75**, 629–636 (2010).
36. Z. L. Wang, G. Z. Li, Z. W. Quan, D. Y. Kong, X. M. Liu, M. Yu, and J. Lin, J. Nanosci. Nanotechnol. **7**, 602–609 (2007).
37. Y. Jin, J. Zhang, S. Lu, H. Zhao, X. Zhang, and X. Wang, J. Phys. Chem. C **112**, 5860–5864 (2008).
38. R. C. De Santana, P. A. Fuentealba, L. J. Q. Maia, V. Paredes-García, D. Aravena, D. Venegas-Yazigi, J. Manzur, and E. Spodine, J. Lumin. **203**, 7–15 (2018).
39. K. Binnemans, R. Van Deun, C. Görller-Walrand, S. R. Collinson, F. Martin, D. W. Bruce, and C. Wickleder, Phys. Chem. Chem. Phys. **2**, 3753–3757 (2000).
40. M. H. V. Werts, *Luminescent lanthanide complexes: Visible light sensitised red and near-infrared luminescence*, Thesis, fully internal, University of Amsterdam, UvA-DARE (Digital Academic Repository), Amsterdam (2000).